Research Square

Preprints are preliminary reports that have not undergone peer review.
They should not be considered conclusive, used to inform clinical practice,
or referenced by the media as validated information.

Failure Mechanisms of Spindle Bearings with High Length-to- Diameter Ratios Induced by Thermal Effects Considering Roughness and Hardness

Li Cui
Shanghai Polytechnic University
Mingkai Chi
Shanghai Polytechnic University
Haoling Wang
Shanghai Polytechnic University
Xin Wang
wangxin2020@126.com

Shanghai Polytechnic University
Ning Li
Shanghai Polytechnic University

Research Article

Keywords: High length-to-diameter-ratio spindle, bearing, roughness, hardness, thermal effect

Posted Date: May 5th, 2026

DOI: https://doi.org/10.21203/rs.3.rs-8307234/v1

License: This work is licensed under a Creative Commons Attribution 4.0 International License.
Read Full License

Additional Declarations: No competing interests reported.

Failure Mechanisms of Spindle Bearings with High Length-to-Diameter Ratios Induced by Thermal Effects Considering Roughness and Hardness

Li Cui[a], Mingkai Chi[a], Haoling Wang[a], Xin Wang[a,*], Ning Li[a]

(a. School of Intelligent Manufacturing and Control Engineering, Shanghai Polytechnic University, 201209, China)

Abstract: To mitigate premature failure in spindle bearings with high length-to-diameter (*L*/*D*) ratios under heavy-duty cutting conditions, this paper incorporates the surface characteristics of the contact microregion into a modified version of the traditional Blok flash-temperature model. The friction–wear behaviors of high-*L*/*D*-ratio spindle bearings with different misalignments were simulated through friction and wear experiments designed under misaligned rolling element-raceway conditions. Comparison of the experimental and numerical results confirmed that the accuracy was more than 20% higher for the proposed model than that for the traditional models at *L*/*D* ratios above 7. The spindle *L*/*D* ratio substantially affected the bearing failure mode under heavy-load cutting conditions. Increasing the *L*/*D* ratio considerably increased the micro area contact stresses and flash temperatures in the bearing, resulting in the risk of early failures such as adhesive failure, rapid initiation, and propagation of subsurface cracks. The flash temperature increased with increasing surface roughness but decreased with increasing hardness. Finally, the transition boundaries between early failure and fatigue failure of the bearings were determined. For spindle bearings with high *L*/*D* ratios and different bearing-precision grades, the surface hardness and surface roughness range must be appropriately selected to prevent adhesion failure and premature subsurface cracking.

Keywords: High length-to-diameter-ratio spindle, bearing, roughness, hardness, thermal effect

* Corresponding author.

E-mail address: wangxin2020@126.com (Xin Wang)

1. Introduction

Bearings in the spindle system experience intense friction between the inner and outer rings under high-speed conditions, generating significant heat. Thermal failure accounts for a large proportion of bearing failures [1]. As mechanical equipment evolves toward higher speeds, heavier loads, and greater precision, increasing thermal loads are imposed on the bearings during operation. The rise in temperature has become a major threat to the performance and service life of spindle systems. Takabi et al. [2] developed a simulation technique that models the impact of thermal expansion of bearings during operation on the contact forces between the components and oil-film thickness. Zhao et al. [3] examined the relationship between the grease friction properties and bearing heat generation, elucidating the lubrication failure mechanism under thermal influence. Bian et al. [4] proposed a thermomechanical bearing model that primarily considers the impact of temperature on the fundamental bearing dimensions. Considering the temperature-induced changes in bearing stiffness, they established a thermal failure model based on stiffness degradation. Macro-level prediction of thermal failure is effective for conventional spindles; however, it is less suitable for deep-hole machining spindles with high length-to-diameter (L/D) ratios, which behave like cantilever beams with considerable deflection under gravity. Under deflection, bearings are subjected to large overturning moments, causing stress concentration. Excessive local contact pressure may rupture the oil film, triggering boundary friction or even dry friction, resulting in thermal failures such as galling, adhesion, or pitting [5]. Accordingly, for deep-hole machining spindles with high L/D ratios, greater attention must be paid to the stress and lubrication conditions within the bearing contact microregion, involving microscopic factors such as bearing roughness and hardness.

Surface roughness and hardness largely affect the thermal failure process of bearings. Roughness is a key characteristic of contact surfaces that directly influences the contact area and heat flux density between friction pairs. Rough surfaces raise the temperature at local contact points, accelerating localized flash heating. Moreover, excessive surface roughness leads to uneven lubricant film distribution and increases the probability of direct metal-to-metal contact, further exacerbating thermal failure [6]. Wang et al. [7,8] demonstrated that bearing roughness considerably affects the relative sliding speed within the bearing contact microregion and the roughness peak-to-load ratio. While excessively low roughness enhances the uniformity of the oil film and prevents direct metal contact, it also increases the relative sliding speed between the rolling elements and raceways, thereby increasing heat generation in the bearings [9].

Hardness, another critical influencing factor, is closely related to the thermal-failure resistance of a material. Typical high-hardness materials are strongly resistant to wear and plastic deformation, and their geometric shape is effectively maintained at elevated temperatures. However, excessively high hardness may increase the material brittleness, particularly under thermal loading where the likelihood of surface crack propagation increases. Insufficient hardness compromises the thermal-fatigue resistance of bearing raceways at elevated temperatures, potentially causing surface scorching and melting. Conversely, excessively hard bearing raceways are prone to premature crack initiation and propagation, ultimately leading to thermal failure. Therefore, the bearing material hardness must be optimized to ensure adequate wear resistance without excessive hardness, leading to thermal fatigue. Chen et al. [10] conducted a finite element analysis of surface and subsurface stresses in bearing raceways. They revealed that case-hardening depth considerably influences for the lifetime of large raceway bearings. Trevisiol et al. [11]

investigated the effects of material hardness, microstructure, and normal load on wear rates. They observed that under high-load conditions, the friction coefficient decreases with increasing hardness and martensite content, thereby improving the failure resistance.

As clarified in the above findings, the surface roughness and hardness nonnegligibly affect thermal failure of bearings. Consequently, traditional thermal failure models that neglect bearing roughness and hardness cannot accurately predict the thermal performance of bearings, necessitating a thermal failure model that accounts for both factors. Vrček et al. [12] investigated micropitting damage on bearing steel with different roughness and hardness values. They revealed that sliding speed and load influence the formation and progression of micropitting. Wang et al. [13] integrated a temperature-dependent isotropic kinematic hardening model with thermal softening, cyclic strain hardening, and damage degradation. Under high-speed cyclic sliding conditions, they showed that transient high temperatures and plastic deformation commonly damage the contact surfaces. However, none of the aforementioned models thoroughly discuss the effects of roughness and hardness on bearing thermal failure or explain the influence of roughness and hardness on the thermal failure mechanism.

This study aims to investigate the influence of bearing surface roughness and hardness on the failure of spindle bearings with high *L*/*D* ratios under unbalanced loads during the machining of conventional materials and cemented carbide. The impacts of different surface parameters on the failure mechanisms of these bearings are also investigated. In particular, the thermal failure process of spindle bearings is systematically characterized under varying surface roughness and hardness conditions. Microfailure mechanisms such as oxidation, crack propagation, and adhesion are observed at elevated temperatures. In addition, the transition boundary between fatigue failure and premature failure in high-L/*D*-ratio spindle bearings is determined under heavy-load cutting operations. Ultimately, this study recommends regulating the bearing surface parameters to prevent premature failure in high *L*/*D*-ratio spindle bearings under heavy-duty cutting conditions.

Nomenclature		a	the major radii of the contact ellipse
F_1	load acting upon the shaft core	b	the minor radii of the contact ellipse
F_2	load acting on the shell	$\sigma_{max,i}$	maximum stress on the *i*-th rolling element
L	span length from the shaft core to the fixed end	f	the traction force
L_h	span from the shell to the fixed end	f_c	centrifugal force on the rolling element
E	elastic modulus of the shaft core	Λ_{lim}	limiting shear stress coefficient
E_h	elastic modulus of the shell	p_h	fluid dynamic pressure
I	moment of inertia of the shaft core cross-section	η_{avg}	average lubricant viscosity
I_h	moment of inertia of the shell cross-section	u_s	relative sliding velocity
θ	relative deflection angle	h_c	central oil-film thickness
θ_s	axis core deflection angle	ΔT	contact micro zone flash temperature
θ_h	shell deflection angle	μ	the coefficient of friction
M	overturning moment	p_m	mean contact pressure at the contact point
K	the angular stiffness of the angular contact ball bearing	L	thermal distribution coefficient

M_x	total overturning moments acting on the bearing about the *x* axes	k	thermal conductivity
M_y	total overturning moments acting on the bearing about the *y* axes	α	diffusivity
i	the i-th rolling element	t_c	contact time
R_m	the pitch circle radius of the rolling elements	A_r	rough peak contact area
Q_{ia}	radial load borne by the i-th rolling element	D	fractal dimension
θ_i	the angular position of the i-th rolling element relative to the reference direction	G	fractal size parameter
N	the total number of rolling elements within the bearing	F_r	load borne by the roughness peaks
Q_i	normal load acting upon the *i*-th rolling element	L_a	the roughness peak-to-load ratio
α_i	contact angle between the i-th rolling element and the raceway	W	dimensionless load number, $W = \frac{Q}{ER^2}$
G	dimensionless material number, $G = E'\gamma$	U	dimensionless speed number, $U = \frac{\eta\mu_e}{E'R^2}$
$\bar{\sigma}$	dimensionless surface roughness number, $\bar{\sigma} = \frac{\sigma}{R}$	V	dimensionless hardness, $V = \frac{v}{E'}$
F_r	load borne by the rough peaks	F_A	the load borne by the contact microregion
H	the hardness	σ_y	yield strength

2. Establishment of Mathematical Models

2.1 Mathematical Model of High length-to-diameter-ratio spindle

Deep-hole machining spindles with very high *L*/*D* ratios exhibit inconsistent bending-deformation trajectories between the shaft core and housing, which deflect the relative angle between the inner and outer rings of the bearing. The relative angular deflection between the shaft core and housing at different positions is calculated from the deflection angle θ_s of the shaft core and the deflection angle θ_h of the shell, respectively, calculated as follows:

$$\theta_s = \frac{F_1 L^3}{6EI}, \tag{1}$$

$$\theta_h = \frac{F_2 L_h^2}{2E_h I_h}, \tag{2}$$

Owing to the interference fit between the bearing inner ring and shaft core and between the outer ring and housing, the deflection angle of the inner and outer rings of the bearing can be equivalent to the relative deflection angle between the shaft core and housing at different positions. Therefore, the relative

deflection angle θ between the inner and outer rings of the bearing is determined as follows:

$$\theta = \theta_s - \theta_h. \tag{3}$$

The overturning moment of a bearing is proportional to θ. The resistance to relative deflection and angular stiffness of a bearing are also related. The angular stiffness of angularly contacting ball bearings ranges from 0.2×10^6 to 1×10^6. The overturning moment M on the bearing is calculated as follows:

$$M = K\theta, \tag{4}$$

As shown in Figure 1, the overturning moment induces eccentric loading on the bearing, resulting in stress concentration in local regions. The total overturning moment is related to the loads borne by all rolling elements as follows [14]:

$$M_x = \sum_{i=1}^{N} M_{ix} = R_m \sum_{i=1}^{N} (Q_{ia} \sin\theta_i), \tag{5}$$

$$M_y = \sum_{i=1}^{N} M_{iy} = -R_m \sum_{i=1}^{N} (Q_{ia} \cos\theta_i), \tag{6}$$

The radial force component on the *i*-th rolling element is

$$Q_{ia} = Q_i \sin\alpha_i, \tag{7}$$

The rolling elements in angular contact ball bearings engage with the inner and outer rings via point contact. According to Hertzian contact theory, the contact stress and normal force are related as

$$Q_i = \frac{2}{3}\sigma_{max,i}\pi a_i b_i, \tag{8}$$

By establishing a mathematical model for deep-hole machining spindles, we can calculate the rolling element loads and stresses caused by eccentric loading at different bearing positions across spindles with varying *L*/*D* ratios, and hence analyze adhesive failure in deep-hole machining spindles.

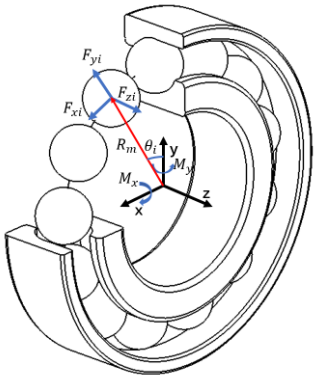


Figure 1. Kinematic model of a bearing

2.2 Effect of Surface Roughness on Flash Temperature

The influence of bearing raceway surface roughness on the seizing resistance of the bearing was investigated as outlined in Wang [7]. Briefly, the bearing motion equations are established and the traction forces at the contact points are evaluated using Masjedi and Khonsari's method [15]. The load on the bearing's microasperities and the sliding velocity are then determined. The traction force f is given by

$$f = \left(Q\frac{L_a}{100}\right)f_c + \Lambda_{lim}p_h\left(1 - \exp\left(\frac{-\eta_{avg}u_s}{\Lambda_{lim}p_h h_c}\right)\right)\pi ab, \tag{9}$$

This method combines the solutions of the bearing motion equation and traction force formula at the contact point to determine the sliding velocity as a function of surface roughness.

The microasperity load ratio denotes the proportion of the total load borne by microasperities relative to the total load across the entire contact interface. Under lubricated contact conditions, the total load on the contact interface is distributed between the lubricating oil film and the surface-contacting microasperities. As demonstrated later, the load borne by the microasperities increases with increasing roughness of the bearing raceway surface.

Although the overall temperature may not exceptionally rise during bearing operation, intense friction between localized microprotrusions on the rolling elements and the directly contacted raceway causes instantaneous flash heating and consequent material softening. When a high-hardness surface passes over a softer surface, the contact surfaces adhere under traction forces, transferring material from the softer to the harder surface. In this paper, the instantaneous temperature rise in the bearing contact microregion is calculated using the Blok flash-temperature model

$$\Delta T = \frac{\mu p_m u_s L}{k^{\pi a t_c}}, \tag{10}$$

Flash temperatures in bearing contact microregions typically occur during bearing operations under boundary lubrication conditions. The temperature at the contact surfaces between the rolling elements and raceways instantaneously rises under high stress at high sliding speeds.

2.3 Effect of Hardness on Flash Temperature

As the actual contact surface is not an ideal smooth plane but contains numerous microasperities, it cannot be described by classical Hertz theory. Multidimensional roughness can be quantified through fractal geometry. Fractal models characterize a rough surface topography in terms of its fractal dimension D, fractal size parameter G, and the fractal upper and lower wavelength limits [16]. Therefore, within the bearing contact ellipse, the rough peak contact area A_r of the contact pair can be expressed as follows:

$$A_r = \left(\frac{D}{2}\right)^{\frac{\frac{D}{2}}{2-D}} a_l^{\frac{D}{2}}\left(\frac{F_r}{K_1 E G^{D-1}}\right)^{\frac{D}{2-D}}. \tag{11}$$

Here, the fractal dimension D typically ranges from 2.0 to 2.5, K_1 combines the coefficients of geometry and elastic mechanics.

For bearings operating under boundary lubrication conditions, the load on the contact microregion is shared between the oil film and the roughness peaks. The roughness peak-to-load ratio is calculated as follows:

$$L_a = 10W^{-0.083}U^{0.143}G^{0.314}[\ln(1+\bar{\sigma}^{4.659}V^{0.509}W^{-0.501}U^{-2.9}G^{-2.87})], \tag{12}$$

Therefore, the load F_r borne by the rough peaks is expressed as

$$F_r = L_a F_A, \tag{13}$$

Some studies have found a relationship between the hardness and yield strength of a material [17]. In general, the hardness H and yield strength σ_y are empirically related as

$$H = \alpha\sigma_y, \tag{14}$$

where α is a constant typically valued between 3 and 4.

The relationship between yield stress and elastic modulus E typically depends on the hardening characteristics, yield criteria, and properties of the material. In many metallic materials, the yield stress and elastic modulus are not directly linearly related but are indirectly linked through the material's yield criteria. In some idealized materials, the yield stress can be approximated as

$$\sigma_y = \beta E. \tag{15}$$

Here, β is a constant typically ranging from 0.01 to 0.1. The specific value of β depends on the properties and hardening behavior of the material. The yield stress of common materials such as steel is usually a small fraction of the elastic modulus. In such cases, the hardness and elastic modulus are related through $E = H/\lambda$, where the magnitude of λ is jointly determined by α and β.

Combining the above equations, we can derive a modified flash temperature model accounting for bearing roughness and hardness. The instantaneous temperature rise in the contact microregion can then be calculated as follows:

$$\Delta T = \mu L \frac{\Lambda_{lim} p_h h_c (F_A L_a)^{\frac{2-2D}{2-D}}}{\eta_{avg} k^{\pi\alpha t_c} \left(\frac{D}{2}\right)^{\frac{\frac{D}{2}}{2-D}} a_L^{\frac{D}{2}} \left(K_1 \frac{H}{\lambda} G^{D-1}\right)^{-\frac{D}{2-D}}} \ln\left(1 - \frac{f - \left(\frac{QL_a}{100}\right) f_c}{\Lambda_{lim} p_h \pi ab}\right), \tag{16}$$

where $L_a = 10W^{-0.083}U^{0.143}G^{0.314}[\ln(1+\bar{\sigma}^{4.659}V^{0.509}W^{-0.501}U^{-2.9}G^{-2.87})]$.

3. Experimental and Simulation Analysis

During actual machining operations, the cutting load borne by the spindle working end is closely

related to the properties of the cut material, such as A36 steel and Ti-6Al-4V titanium alloy. When machining conventional metal materials, the cutting force on the spindle front end typically ranges between 100 and 300 N, indicating light-load cutting conditions. In contrast, when machining high-strength or super-hard materials, the cutting force often reaches 400–600 N, typifying heavy-duty cutting. Thus, the material conditions can markedly alter the loads borne by the spindle end during the cutting process. To verify the impact of roughness and hardness on bearing failure in spindle bearings with high *L*/*D* ratios under cutting forces, the present authors designed a ball–disc friction and wear test that can accommodate unbalanced loads. The contact between the rolling elements and raceways in deep-hole machining spindle ball bearings is simulated on a ball–disc friction pair (see Figure 2(a)). The test variables were altered by modifying the surface roughness and hardness of the annular specimen. As bearing rolling elements are typically harder than their raceways, the test bearings were formed from silicon nitride ceramic. This choice not only meets the requirement of different hardnesses but also minimizes the impact of contact area changes on the ball's contact surface during friction and wear tests. The rotational speed was derived from the calculation model of relative sliding speed established above. As the test ball does not spontaneously rotate within the ball–disc friction pair during the grinding process, the calculated relative sliding speed can be directly applied to the grinding head. This study investigates the influence of the load borne by roughness peaks on adhesive failure. Under identical external loads, the roughness peak load in the mathematical model correlates with the surface roughness magnitude. Therefore, during the experiments, the surface roughness of the annular specimens was varied to control the peak load distribution while maintaining a constant force across groups. As shown in Figure 3, the inclination angle of the specimen mounting plate was controlled by rotating the threaded rod on the friction and wear testing machine, in conjunction with the force sensor readings. The research subject was a precision-machined spindle. To ensure high machining accuracy, high-precision-grade bearings were selected. Considering the actual application scenarios of spindles, the bearing accuracy grades within the scope of this study are P2, P4, and P5. According to relevant standards, the surface roughness range for bearings of these accuracy grades typically falls between 0.01 and 0.09 μm. Unbalanced loading caused varying degrees of wear on the specimen surface (Figure 2(b)), with more severe wear on the off-center loading zone.

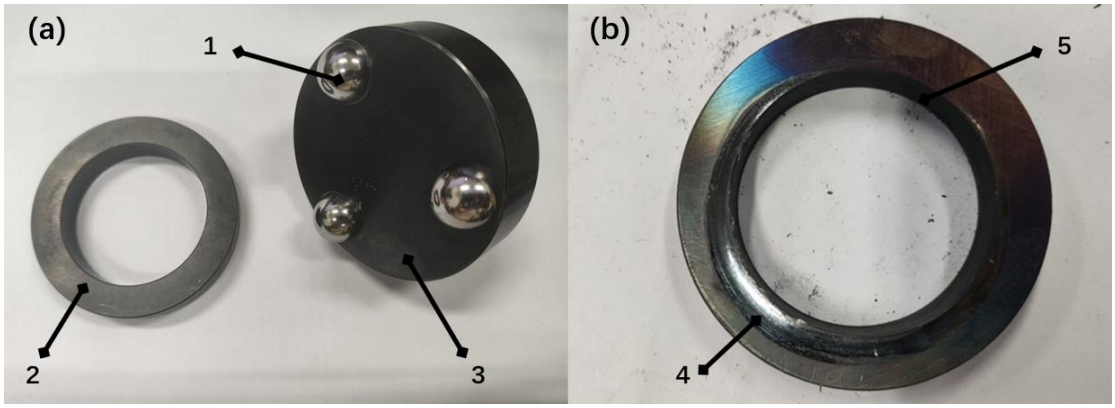


Figure 2. Ball–disc friction pair: (a) assembly of the ball–disc friction pair and (b) demonstration of the

off-center loading effect; (1 Test Ball; 2 Test Specimen; 3 Test Ball Mounting Disc; 4 Highly loaded Area; and 5 Low loaded Area during Off-Center Loading)

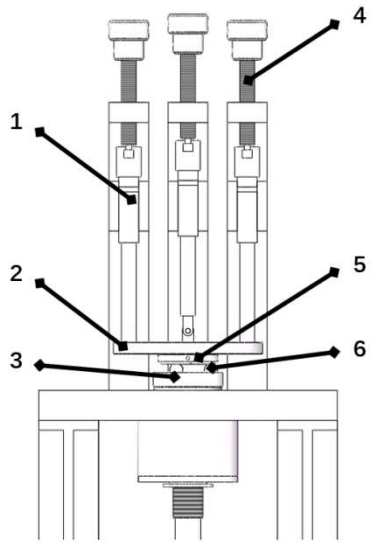


Figure 3. Friction-and-wear test bench (1 Force Sensor; 2 Specimen Mounting Plate; 3 Test Ball Mounting Plate; 4 Threaded Rod; 5 Specimen; and 6 Test Ball)

The hardness of the specimens used in this study was determined via nanoindentation testing. Nanoindentation is an experimental technique employed to measure material hardness, elastic modulus, and other mechanical properties. It involves applying a minute load to the material surface using a diamond indenter with an extremely small radius, while recording the relationship between the applied load and the resulting indentation depth. This process is applicable to a wide range of materials, including metals, ceramics, thin films, polymers, and composites. The hardness unit HRC used in this article refers to the Rockwell C scale method for measuring material hardness, commonly employed to evaluate the wear resistance and strength of metallic materials.

The specimens were observed using scanning electron microscopy (Zeiss Sigma 300 SEM; Carl Zeiss AG, Germany) with a magnification range of 10× to 1,000,000×. The friction raceway surfaces were observed at 100× to 200× magnification whereas the planed specimen surfaces were observed at 2,000× to 5,000×. The elemental compositions of the friction raceway surfaces were observed using energy dispersive X-ray spectroscopy (EDS).

To validate the bearing imbalance caused by cutting forces in spindles with high L/D ratios, an equivalent model of such spindles was established in ROMAX Designer software. In this model, the inner and outer rings of the bearing are connected to the shaft core system and the sleeve system (housing diameter 200 mm), respectively. To further analyze the impact of L/D ratio on the maximum bearing stress state, whether to incorporate gravitational forces must be considered because gravity causes bending deflection differences between the spindle housing and shaft core, which substantially affect the stress distribution. When setting the boundary condition, a uniformly distributed working load was applied at the front end of the spindle where the grinding wheel is mounted. The structural model of the high-L/D-ratio spindle is shown in Figure 4.

The materials of the long-stroke spindle system are listed in Table 1.

Table 1 Parameters of the Spindle System Materials

Name	Density (t/mm³)	Modulus of elasticity (MPa)	Poisson ratio
Shaft core	7.85×10^{-9}	2.09×10^{5}	0.272
Sleeve	7.85×10^{-9}	2.06×10^{5}	0.27
Bearing	7.85×10^{-9}	2.07×10^{5}	0.3

Based on the structural diagram of the high-*L*/*D*-ratio spindle, the bearing positions of the spindle housing were mounted with PT100 temperature sensors as shown in Figure 5. The monitoring range of the sensor (–50°C to 500°C) sufficiently covers the temperature variations during spindle operation. To monitor the temperature changes in each bearing group, temperature sensors 1–6 were affixed to their corresponding bearing assemblies 1–6. The temperature variations of each bearing group were recorded on the display for comparison with the calculated flash temperature results.

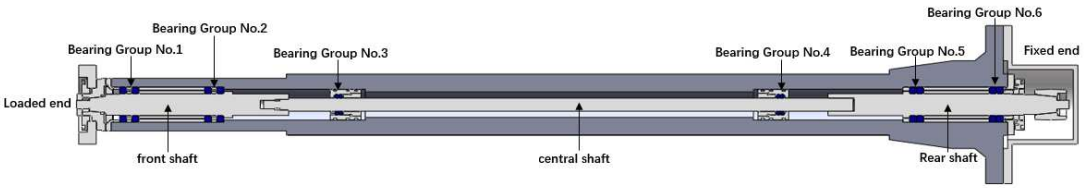


Figure 4. Schematic of the spindle structure

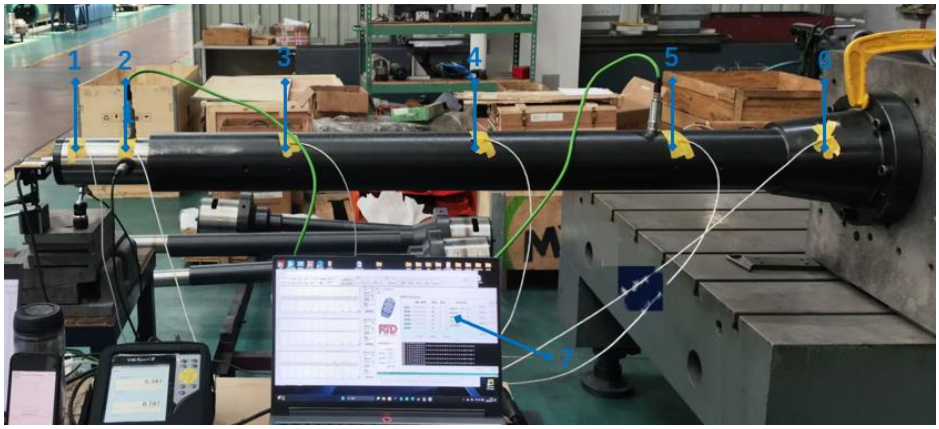


Figure 5. Spindle temperature test platform (1 Sensor 1; 2 Sensor 2; 3 Sensor 3; 4 Sensor 4; 5 Sensor 5; 6 Sensor 6; and 7 Temperature Monitoring Interface)

As metal materials are heat-treated during the manufacturing of bearing components, the material properties differ between the surface and subsurface layers of the bearing raceway. The hardened layer is approximately 200 μm deep. When simulating bearing crack initiation, this paper defines one-fifth of the hardened-layer depth as the surface layer and the remaining four-fifths as the subsurface layer (Figure 6). The finite element model divides the structure into layers that gradually thicken from the surface layer inward. The material properties of each layer depend on the contents of the microstructural components in that layer. After heat treatment, the martensite content decreases from the surface layer to the interior.

The contents of the other components also vary with depth [18]. Multiple simulations and literature reviews have indicated that under cyclic loading, cracks frequently initiate in the subsurface layer because the highest shear stresses typically develop in this region. As cracks first propagate along the direction of maximum shear stress, these locations are the primary crack initiation sites [19]. The influence of carbides must also be considered, as carbides tend to concentrate stress, favoring crack initiation in carbide regions [20]. Through finite element calculations and contour plots, the load boundary at which subsurface cracks will likely form within the bearing's rated life can be verified in subsurface regions with varying roughness and hardness.

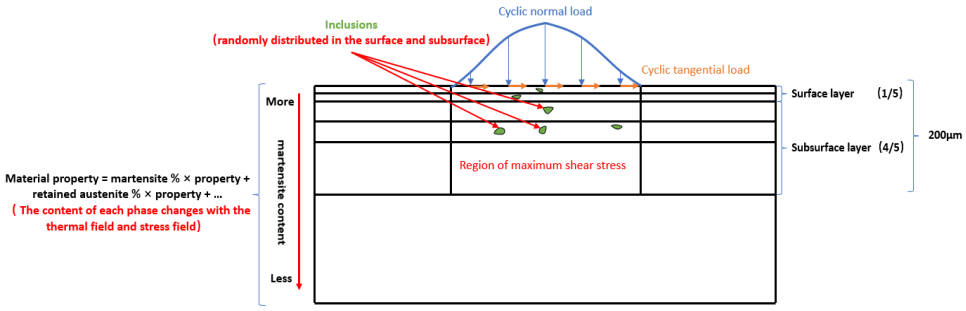


Figure 6. Schematic of the finite element simulation

4. Results and Discussion

4.1 Influence of Spindle Length-to-Diameter Ratio on Bearing Failure Modes

The rear bearing of spindles with a high *L/D* ratio is positioned near the fixed end, where deformation is structurally constrained. The front bearing, at the loaded end with substantial overhang from the fixed end, exhibits low structural stiffness and experiences the greatest relative tilt angle. This study analyzed seven Romax-built models with the same spindle outer diameters of 200 mm and varying spindle lengths in the range of 400–2800 mm. Based on the calculations of spindle outer diameter and length dimensions, the equivalent *L*/*D* ratio ranged from 2 to 14. Figure 7 shows the analysis results. Increasing the spindle length increases the relative inclination angle of the front bearing, consequently increasing the bearing misalignment and imposing higher loads on the rolling elements. The local stresses within the bearing are then elevated. As such high-*L*/*D*-ratio spindles structurally resemble a cantilever beam, excessive bending deflection is primarily caused by gravitational forces. Whether gravitational effects should be considered was determined through a comparative simulation of bearing misalignments in spindles with different high *L*/*D* ratios. When gravity was considered, the maximum stress on the bearing increased by 164.8% as the spindle *L*/*D* ratio increased from 2 to 14. However, when gravity was excluded, the maximum stress on the bearing increased by only 59% under the same spindle *L*/*D* ratio increase. This result demonstrates that as the spindle length increases, the *L*/*D* ratio increasingly exacerbates the unbalanced-load-induced stress concentration in bearings [21], confirming the importance of unbalanced load on the bearing life of high-*L*/*D*-ratio spindles under heavy-duty cutting conditions. The bearing raceway contact load derived from the simulation analysis was adopted as the test force in the friction and wear test.

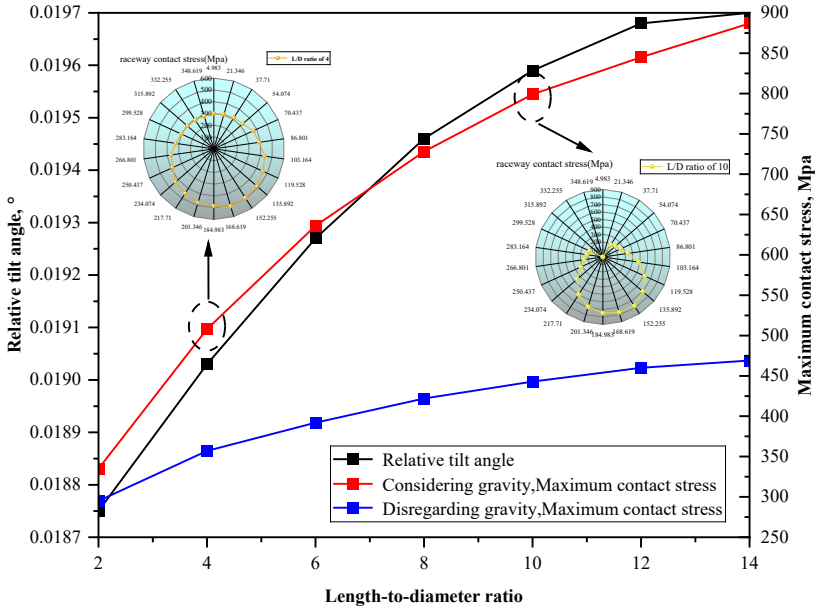


Figure 7. Effect of spindle length-to-diameter (L/D) ratio on the relative inclination angle between the bearing inner and outer rings (left axis) and maximum contact stress on the raceway (right axis)

Traditional flash temperature models consider macroscopic relative sliding velocity and contact pressure. The relative sliding velocity is derived from the bearing motion equations, and the contact pressure is obtained from the Hertzian contact theory. Consequently, all inputs to conventional models are macroscopic bearing parameters, neglecting the influence of microscopic factors such as roughness and hardness. Therefore, the traditional model predicts identical flash temperatures under the same external loads, rotational speeds, and geometric parameters. In actual situations, the flash temperature can vary under different surface conditions.

By contrast, the proposed model incorporates roughness and hardness factors to more accurately characterize the influence of microsurface conditions on flash temperature. As shown in Figure 8(a), the calculated values of this model increasingly exceed those of the traditional model as the surface roughness increases. Moreover, the difference between the two models becomes more pronounced with increasing spindle L/D ratio. At an aspect ratio of 10, the roughness variation increases the discrepancy between the two models to 30%. Decreasing the hardness also increases the discrepancy between the proposed and traditional models. Again, this difference becomes more pronounced with increasing L/D ratio (Figure 8(b)). Therefore, in addition to directly influencing the flash temperature results, the roughness and hardness parameters interact with the L/D ratio to amplify the computational differences between the traditional and improved models.

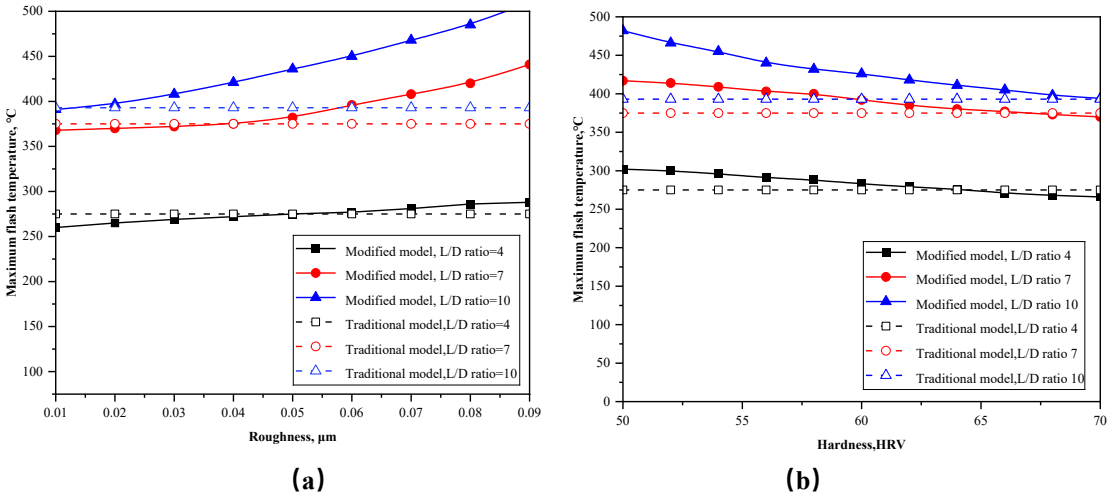


Figure 8. Effects of (a) roughness and (b) hardness on the flash temperatures calculated using the traditional model and model proposed in this paper.

The temperature variations across various bearings were monitored using a spindle-temperature testing device. The monitoring results were compared with the flash temperature outcomes calculated using the roughness-considering flash-temperature failure model. The recorded instantaneous flash temperatures in the contact microregion were largely consistent with the model results (Figure 9(a)), further demonstrating that increased roughness elevates the flash temperature within the contact microregion. Figure 9(b) displays the instantaneous temperature variations recorded during 1 s of the stable operation of bearings with different hardness levels under identical loads. Increasing the hardness gradually decreases the instantaneous temperature in the contact microregion. Furthermore, the recorded results are consistent with the instantaneous maximum temperatures calculated by the established mathematical model, validating the accuracy of the flash-temperature failure model. Therefore, bearing roughness and hardness are required for accurate flash-temperature calculations in bearing contact microregions.

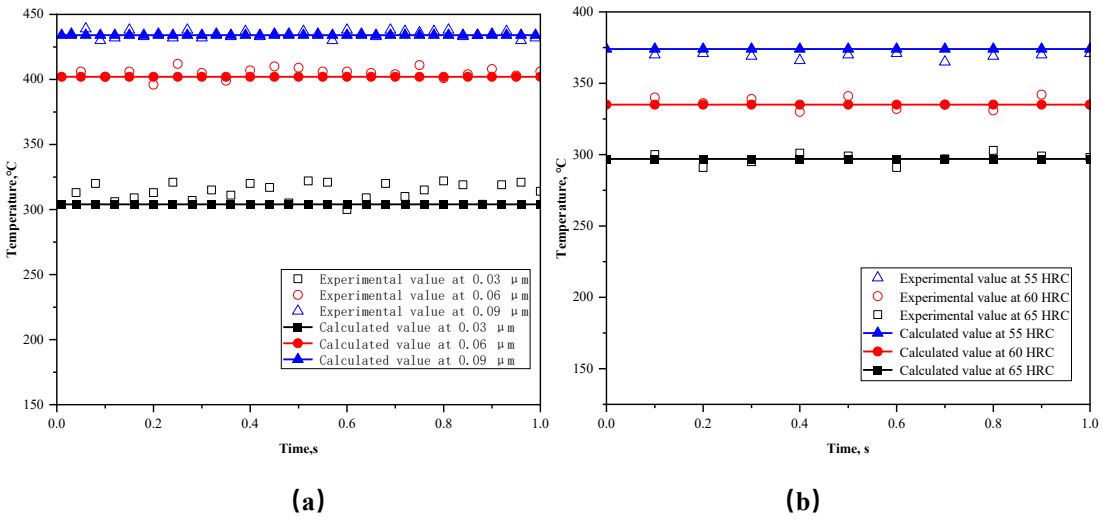
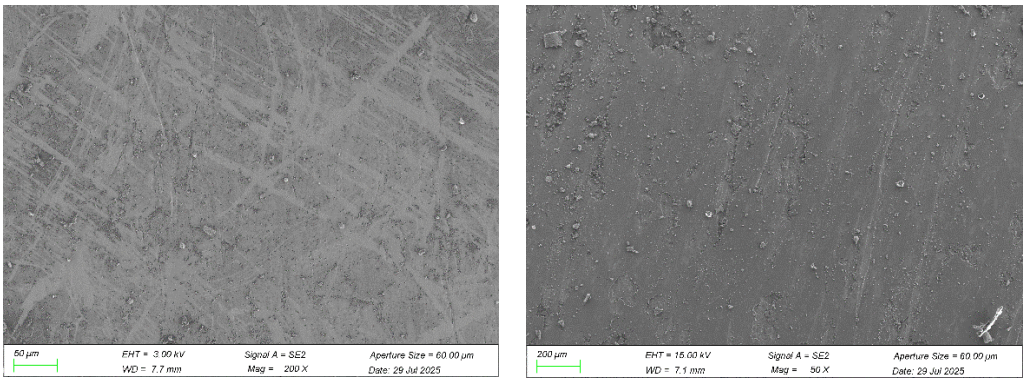


Figure 9. Transient temperature changes within 1 s under (a) different roughness conditions and (b) different hardness conditions.

The friction and wear tests were performed under two load-stress conditions: one considering and one disregarding the influence of *L*/*D* ratio. The failure modes under the two conditions were compared in

SEM images and cross-sections of the specimen raceway surfaces. Figures 10 and 11 show the friction-wear patterns on the raceway specimens after disregarding and considering the *L*/*D* ratio, respectively. For spindles of the same length, disregarding the *L*/*D* ratio considerably improves the wear condition on the raceway surface from that of the specimen tested under the *L*/*D*-ratio condition. Comparing Figure 10(b) and Figure 11(f), it is evident that under load conditions calculated for a spindle length-to-diameter ratio of 10, significant adhesive failure has already occurred on the raceway surface when unbalanced loads are considered. In contrast, under load conditions calculated for a spindle length-to-diameter ratio of 14, only minor banded spalling appears on the raceway surface when the effect of gravity on the length-to-diameter ratio is disregarded. Therefore, the unbalanced load caused by an excessively high length-to-diameter ratio cannot be ignored in bearing failure analysis.

Panels (a) and (b) of Figure 11 show the raceway surface and its cross-section, respectively, at an *L*/*D* ratio of 7. A short crack appears in the subsurface layer. When the *L*/*D* ratio is less than or equal to 7, the bending deflection of the spindle is small; therefore, the relative inclination angle between the inner and outer rings is also small. Consequently, the stress concentration in the bearing is reduced and a low contact stress is imposed on the bearing microcontact zone. The flash temperature is minimal, and the oil film remains stable. The roughness peaks of the mating surfaces within the microcontact zone remain separate, thus preventing peak adhesion. Only minor shear stresses form in the subsurface layer, ultimately leading primarily to fatigue failure [22]. When the spindle *L*/*D* ratio is larger than 7 but smaller than 10, the intensified stress concentration induces higher shear stresses in the subsurface layer that accelerate crack initiation and propagation to the surface (Figure 11(c) and (d)). The elevated stresses also raise the micro area flash temperatures, reducing the material hardness and increasing the crack propagation speed. Under substantial tangential loads, the crack initiation aligns with the relative sliding velocity direction, resulting in predominantly banded spalling of the bearing raceway [23]. At a spindle *L*/*D* ratio of 10 or higher, excessive relative inclination angles between the inner and outer rings can remove the load from some rolling elements, inducing severe stress concentration, increasing the microcontact zone flash temperatures, and destabilizing the oil film. The material exhibits pronounced tempering softening, resulting in roughness adhesion between the mating surfaces and in adhesive failure [24,25] (Figure 11(e) and (f)). Although the shear stresses are raised in the subsurface layer, the excessive temperatures and contact stresses prevent the propagation of subsurface cracks to the surface before adhesive failure occurs.



(a) **(b)**

Figure 10. SEM images of specimen raceway surfaces after the friction and wear test not considering

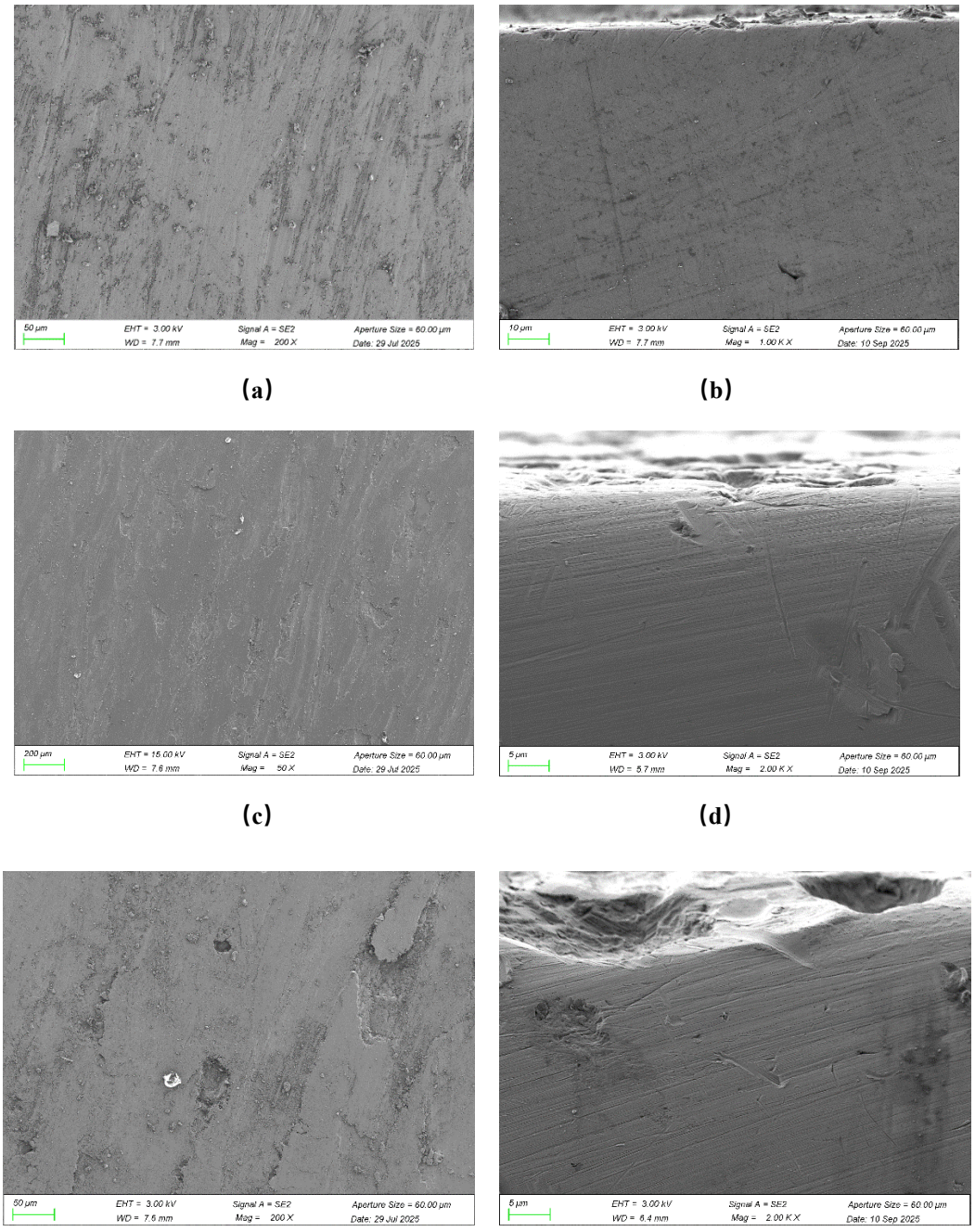


Figure 11. SEM images of the specimen raceway surfaces (left) and raceway cross-sections (right) for spindles with aspect ratios of 7 (a) and (b), 9 (c) and (d), and 10 (e) and (f) after the friction and wear test considering the aspect ratio (i.e., unbalanced loads)

4.2 Influence of Bearing Surface Parameters on Failure

Figure 12 shows the calculation results of the above-established flash temperature model. Increasing the roughness decreases the relative sliding speed between the bearing rolling elements and raceway, increases the load-bearing ratio of the roughness peaks in the contact microregion, and raises the instantaneous flash temperature in the contact microregion. Meanwhile, increasing the hardness decreases the instantaneous flash temperature. As documented in Shi [26], the flash temperature is jointly

determined by the relative sliding speed and contact pressure. As the relative sliding speed and roughness peak-to-load ratio exhibit opposite trends with increasing roughness, the thermal failure modes in bearings differ under varying roughness conditions. Failure can be dominantly caused by excessive relative sliding speed or excessive contact pressure.

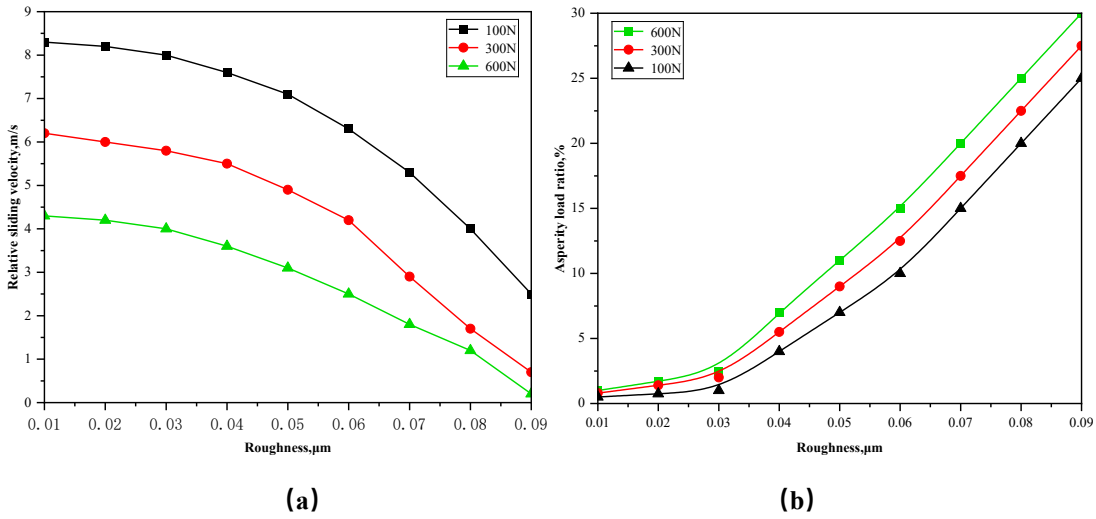


Figure 12. Relationships between roughness and (a) relative sliding velocity and (b) roughness-peak load ratio.

Figure 13 shows the results of the friction and wear tests on the specimens under different roughness conditions. The flash temperature in the contact microregion considerably lowers with decreasing roughness. Under a 100-N load, reducing the roughness alone reduces the flash temperature by 71.4%. However, increasing the load gradually reduces the regulatory effect of roughness on the flash temperature. Under a load of 600 N, reducing the surface roughness reduces the flash temperature by only approximately 5% (Figure 13(a)), indicating that under high-load conditions, optimizing the roughness alone cannot effectively enhance the thermal-failure resistance. Further experiments controlling the hardness under 400, 500, and 600 N loads yielded the results shown in Figure 13(b). Increasing the material hardness considerably reduces the flash temperature by approximately 70%, 46%, and 45%, respectively.

Intense friction and contact stresses in the microcontact zones generate instantaneous high temperatures, promoting high-temperature oxidation reactions between the surface and atmospheric oxygen [27]. Oxidation wear in microcontact zones is often accompanied by adhesive failure [28]. Decreasing the roughness diminishes the flash temperatures and oxygen content on the raceway surface, indicating weakening of the thermal oxidation reactions. Herein, the sliding pair material was silicon nitride ceramic. Table 2 presents the EDS results of the raceway surfaces of the specimens with adjusted roughness under high and low loads. Under low loads, reducing the roughness decreases the contents of detected Si and O elements on the raceway surface. This result can be elucidated by the reduction of contact stress between the diminished roughness peaks, weakening the adhesion effect and consequently lowering the Si content. Reducing the roughness also decreases the flash temperature in the contact microregion, thereby mitigating the extent of oxidation reactions. Thus, reducing the roughness alone can substantially enhance the thermal-failure resistance of the bearing under low-load conditions. However, under higher loads, the Si and O contents are not prominently reduced, further clarifying that reducing the roughness alone cannot substantially improve the thermal-failure resistance of the bearing.

Under cyclic loading, the contact microregion of this bearing is subjected to both work hardening and material softening [29-32]. Figure 13(b) shows the results of the nanoindentation tests on specimens of varying hardness. Cyclic loading actually increases the hardness of the specimen with an initial hardness of 70 HRC, indicating that the work-hardening effect induced by cyclic loading outweighs the softening effect. When the initial hardness is 60 HRC, the surface hardness effect. At an initial hardness of 50 HRC, the surface hardness notably decreases because the excessively low hardness increases the flash temperature, allowing the tempering softening effect to dominate the work hardening effect. Therefore, the high-hardness specimen remains stable while reducing the flash temperature.

Table 2 Comparison of Surface Element Content in Test Specimen Raceways with Different Roughness Values

Element Name	P2, Element Content (%) Load 100 N	P2, Element Content (%) Load 500 N	P5, Element Content (%) Load 100 N
C	11.52	7.64	8.57
O	9.78	29.64	29.58
Al	0.20	0.25	0.40
Si	0.36	1.98	3.05
K	0.09	0.12	0.20
Cr	1.28	0.98	1.07
Mn	0.24	0.30	0.27
Fe	75.61	59.10	56.76

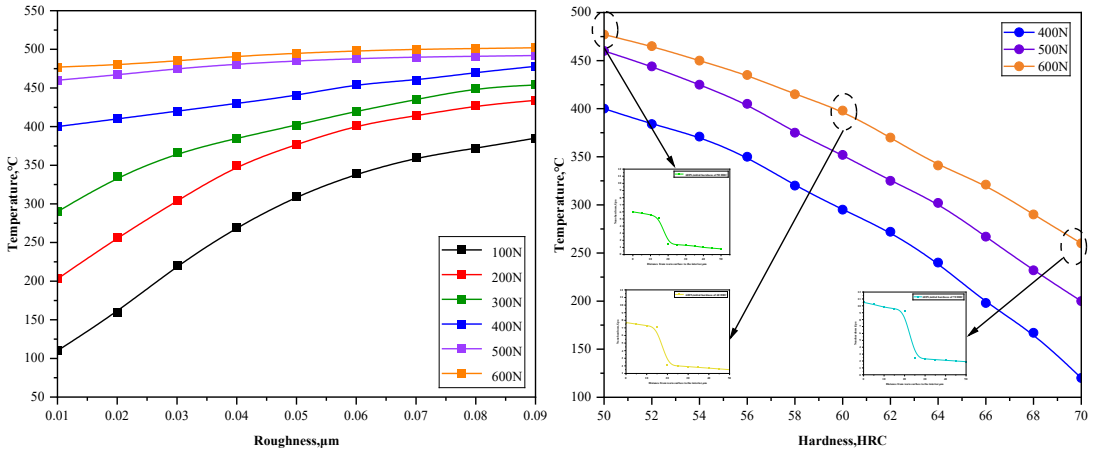
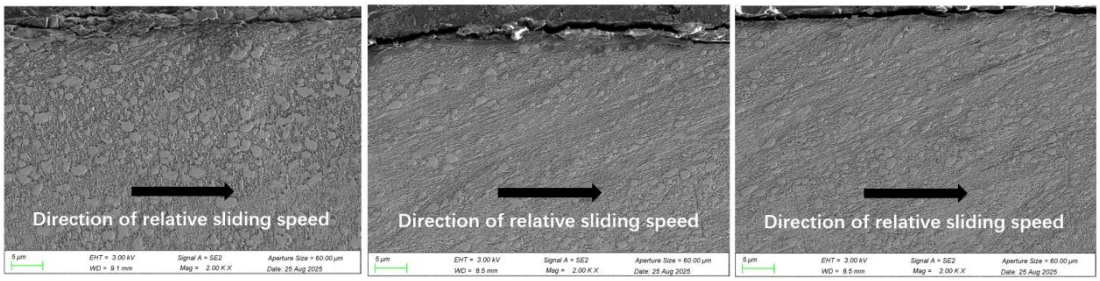


Figure 13. Effects of (a) roughness on flash temperature under different load conditions and (b) hardness on flash temperature.

The aforementioned conclusions are corroborated by the SEM cross-sections in Figure 14. Severe plastic flow, aligning along the slip direction, occurs in the surface layer and subsurface layer of the lower-hardness specimens. As the hardness increases, the plastic flow gradually diminishes and almost no discernible subsurface flow lines appear at 70 HRC. Increasing the hardness impedes dislocation slip, thereby raising the crack initiation threshold in the subsurface layer and suppressing spalling occurrence.



(a) **(b)** **(c)**

Figure 14. SEM images of the friction-affected layer on specimens with different hardness values: (a) 70 HRC, (b) 60 HRC, and (c) 50 HRC.

Increasing the hardness can also reduce the likelihood of adhesive failure because high flash temperatures induce martensitic tempering softening (Figure 15). During this process, carbon atom precipitation induces gradual coarsening and lamellar formation of carbides [33]. As the temperature increases, these lamellar carbides start dissolving into fine spherical carbides, which migrate toward the martensite boundaries and aggregate into larger spherical carbides (Figure 15). Accordingly, the hardness exhibits a "decreasing–stable–decreasing" trend [34]. Around 600°C, high-carbon chromium bearing steel also enters the low-temperature brittleness zone, where carbide aggregation further increases the crack initiation sensitivity [35]. Cross-sectional observations (Figure 16) reveal numerous lamellar carbides on the 70 HRC surface, indicating incomplete tempering and limited hardness reduction. High hardness maintenance prevents any notable increase in the flash temperature. At this stage, the carbide particles are small (submicron-sized) and suppress the initiation and propagation of subsurface cracks, thus enhancing the fatigue performance [36-38]. The 60 HRC specimen is also distributed throughout with spherical carbides, with its hardness remaining stable at a lower level. By contrast, the 50 HRC specimen exhibits agglomerated spherical carbides at the grain boundaries. The grains near these carbide clusters are subjected to localized plastic strain, which indicates a precursor of fatigue cracking [39]. Furthermore, the hardness of this sample is markedly reduced by martensitic tempering softening. According to the established mathematical model, such softening will increase the flash temperature, initiating a vicious cycle that substantially elevates the risk of thermal failure.

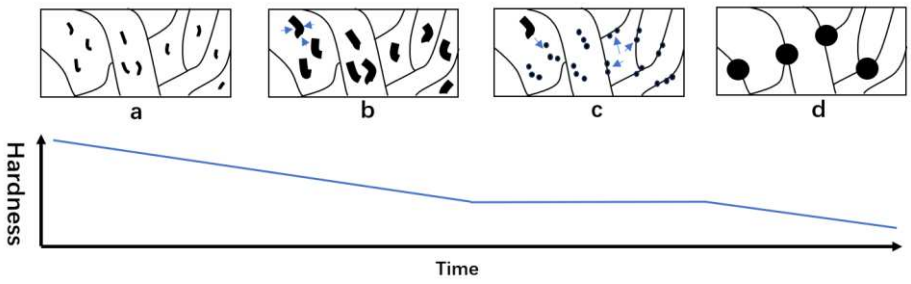


Figure 15. Schematic of martensite tempering softening

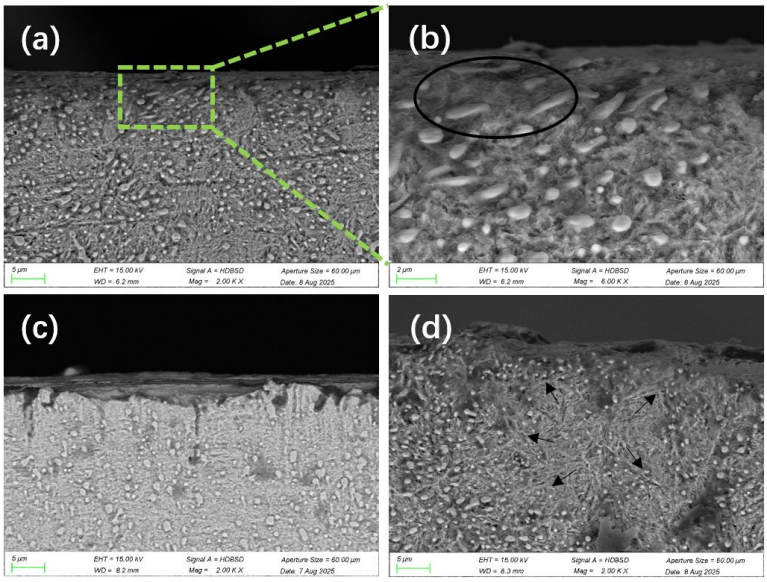


Figure 16. SEM cross-sectional images of specimens with different hardness values: (a) carbide morphology and distribution in the cross-section of the 70 HRC specimen; (b) localized enlargement of the 70 HRC specimen. Morphologies and distributions of carbide in (c) the 60 HRC specimen and (d) 50 HRC specimen.

As shown in Figure 17, reducing the surface roughness effectively reduces the flash temperature under light-load cutting conditions; however, optimizing the roughness alone yields limited improvement under heavy-load cutting conditions. To improve the performance under such conditions, the roughness and hardness must be concurrently optimized. Moreover, under heavy-load cutting conditions, high flash temperatures cyclically deteriorate the material properties. In addition to reducing the flash temperature, high hardness is degradation resistant and minimizes the occurrence of plastic flow.

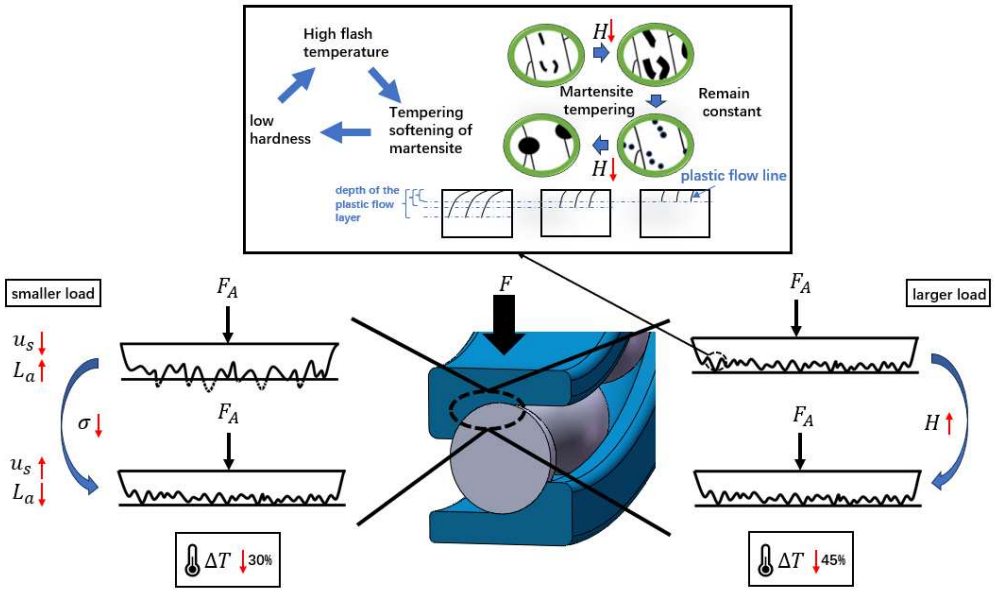


Figure 17. Thermal effects in bearing contact microregions under roughness and hardness considerations

4.3 Failure Boundary Analysis

Further analysis revealed that roughness and hardness in different failure modes are not independent but exhibit considerable interactive effects (Figure 18). Overall, increasing the roughness markedly increases the critical load beyond which surface cracks easily initiate and propagate, indicating that rough surfaces can mitigate early crack formation to some extent. However, high roughness considerably reduces the critical load of adhesive failure, substantially increasing the risk of thermal adhesion and localized fusion welding on the surface.

As the hardness increases, the critical load of subsurface cracks leading to premature failure trends completely opposite to that of roughness. High hardness effectively enhances the plastic flow and shear slip resistance of the material, suppressing rapid crack initiation and propagation in the subsurface layer while reducing the flash temperature level in the contact microregions. Therefore, the likelihood of thermal adhesion and localized fusion is diminished and the probability of adhesion failure lessens, even on rough surfaces. In conclusion, increasing the hardness can largely offset the risks associated with increasing roughness.

This pattern can be quantified using the above-established finite element model. According to the model calculations, the contact stresses are maximized on the bearing raceways of spindles with varying *L*/*D* ratios. These findings can be combined with the contact area data to determine the load magnitude on the rolling elements. Comparing these results with the experimental boundaries in Figure 18, the roughness–hardness parameter boundaries were established under different conditions (Figure 19). Within these boundaries, the bearing is protected from rapid initiation and propagation of subsurface cracks and adhesive failure at different *L*/*D* ratios. Panels (a), (b), and (c) of Figure 19 present the light-load cutting boundaries for spindle *L*/*D* ratios of 4, 7, and 10, respectively; panels (d)–(f) of Figure 19 present the corresponding boundaries under heavy-load cutting conditions under the same *L*/*D* ratios. Spindles with high *L*/*D* ratios must be designed under specific machining-accuracy requirements, and some P5-grade bearings fail to meet the operational demands. This design constraint must be considered when selecting the bearing parameters. At a spindle *L*/*D* ratio of 4, a hardness of 62 HRC or higher will guarantee the functioning of precision grade P2, P4, and P5 bearings throughout their service life under light- and heavy-load cutting conditions. As 62 HRC is a common manufacturing hardness for bearings, no additional hardness requirements are imposable at this *L*/*D* ratio. When the spindle *L*/*D* ratio increases to 7, bearings of all precision grades can avoid premature failure within the hardness range achievable by conventional manufacturing processes under light-load conditions. However, under heavy-load cutting conditions, only bearings with higher surface roughness remain stable at conventional hardness levels. P2-grade bearings with lower surface roughness require further hardness enhancement to effectively suppress premature failure. When the spindle *L*/*D* ratio further increases to 10, the conditions become more severe. To protect all precision grades from premature failure under heavy-load cutting, the hardness must be substantially increased beyond the requirements of *L*/*D* ratio = 7. Notably, even P2-grade bearings with 70 HRC hardness but lower surface roughness may fail to meet the service requirements. Therefore, when applying a spindle with a 10:1 *L*/*D* ratio to heavy-load cutting, the bearing roughness and hardness matching must be strictly controlled, highly raising the manufacturing and design requirements.

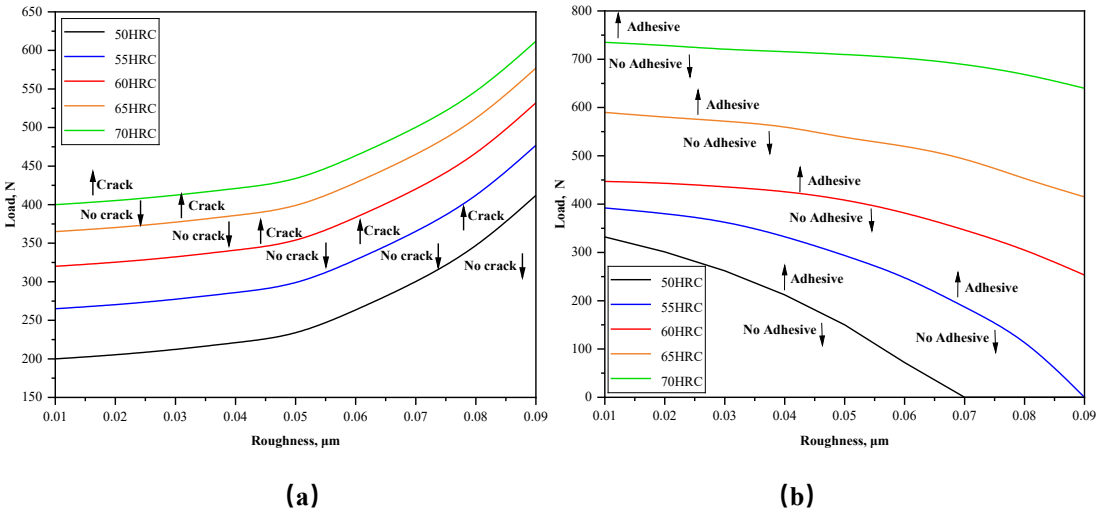


Figure 18. Effects of roughness and hardness on (a) failure caused by subsurface cracks and (b) adhesive failure.

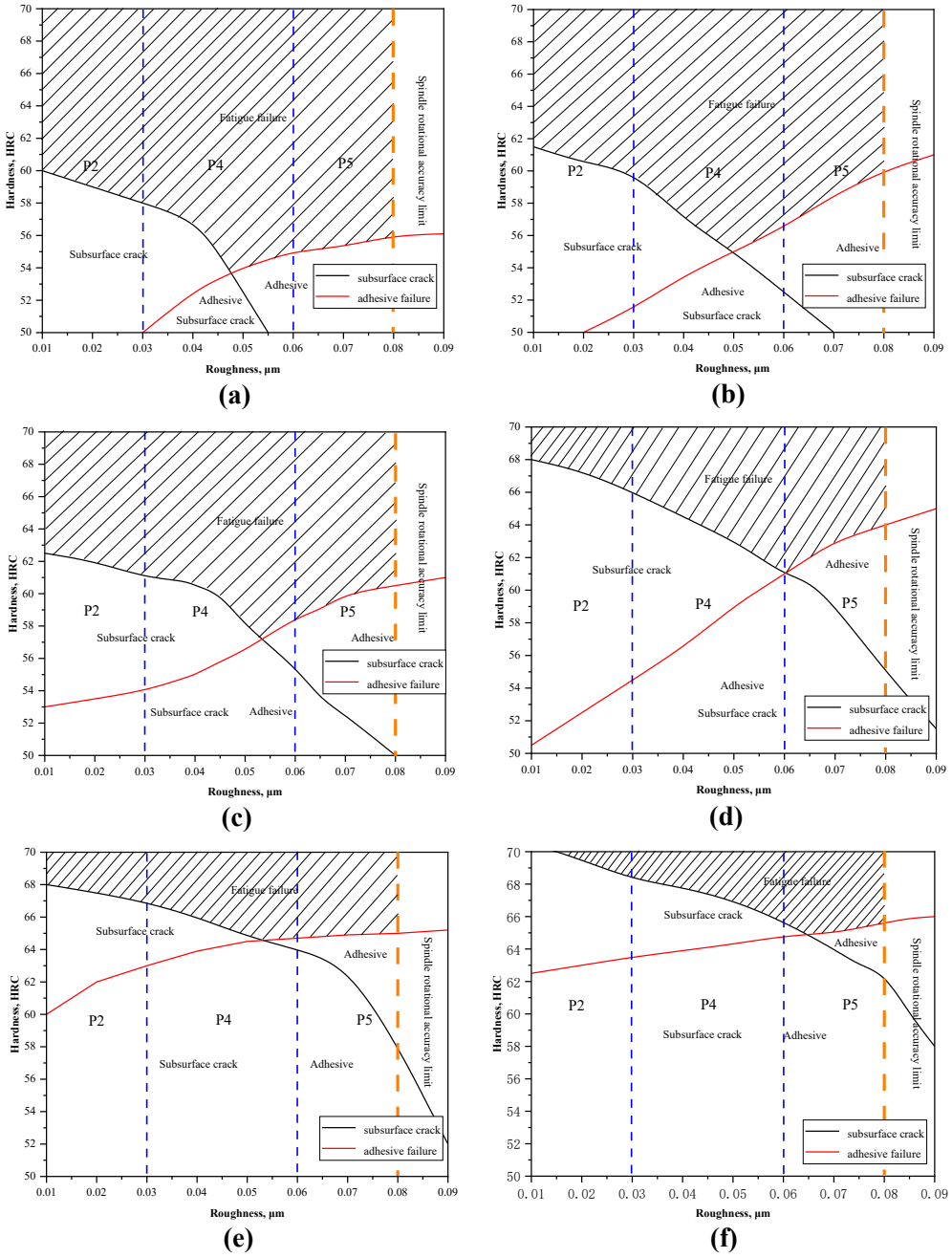


Figure 19. Boundaries at which the bearings are safe from premature failure under light and heavy loads for spindles with different *L*/*D* ratios: (a) light load, *L*/*D* ratio = 4; (b) heavy load, *L*/*D* = 4; (c) light load, *L*/*D* = 7; (d) heavy load, *L*/*D* = 7; (e) light load, *L*/*D* = 10; (f) heavy load, *L*/*D* = 10.

5. Conclusion

This study investigated thermal failure of bearings in spindles with high *L*/*D* ratios owing to eccentric loading. Building upon the traditional Blok flash-temperature failure model, a modified flash temperature model that accounts for the dual roughness–hardness effects on the instantaneous temperature rise was developed. This approach explores the effects of roughness and hardness on the bearing failure modes

and elucidates the thermal failure mechanism in spindle bearings with high L/D ratios. The following conclusions were drawn from this study.

1. Heavy-load cutting conditions substantially increase the relative inclination angles of the bearings in spindles with high L/D ratios, markedly intensifying the unbalanced load effect and causing localized bearing stresses and transient flash temperatures. As the L/D ratio increases from 2 to 14, the maximum bearing stress progressively increases to 165% of its original value. Based on these data, a flash temperature failure model incorporating the roughness and hardness factors was developed. This model accurately reveals the influence of microsurface conditions on the instantaneous contact temperature rise. The calculated results were validated through experiments against the measured data. Friction and wear experiments on spindles with high L/D ratios revealed different primary failure modes during heavy-load cutting: surface-crack-induced fatigue failure at L/D ratios ≤ 7, crack initiation and propagation to the surface accelerated by stress concentration and elevated flash temperatures at $7 < L/D$ ratio < 10, resulting in rapid subsurface crack growth culminating in early fatigue failure, and adhesive failure at L/D ratio ≥ 10, where excessive relative inclination angles between the inner and outer rings increase the microzone flash temperatures and cause material tempering softening. Adhesion between the roughness peaks results in adhesive failure.

2. As clarified in the flash temperature calculation model, roughness and hardness considerably influence the instantaneous flash temperature and failure modes within the bearing contact microregion. Decreasing the roughness and increasing the hardness considerably decrease the flash temperature in the contact microregion, effectively reducing the likelihood of adhesive failure. Increasing the hardness enhances the stability of raceway hardness and helps to suppress the initiation and propagation of subsurface cracks. By contrast, reducing the roughness increases the relative sliding speed between the rolling elements and raceways, elevating the subsurface shear stresses that accelerate crack initiation and propagation.

3. Roughness and hardness substantially affect the early-stage bearing failure modes. Increasing the roughness increases the critical load of rapid subsurface crack initiation and markedly reduces the critical load of adhesive failure. Conversely, increasing the hardness effectively suppresses subsurface crack propagation and reduces the flash temperature, thereby mitigating the risk of adhesive failure. Comparing the results of finite element calculations and experiments at varying L/D ratios under different load conditions, higher L/D ratios were observed to demand higher-hardness bearings under heavy-load cutting. At an L/D ratio of 4, early bearing failure can be prevented over a broad range of roughness and hardness values. When the L/D ratio increases to 7, the surface hardness must be slightly increased under light-load conditions and substantially increased under heavy-load conditions. When the L/D ratio further increases to 10, the bearing surface hardness must be largely elevated, especially for high-precision bearings where the surface hardness design becomes critically important. Overall, for spindles with high L/D ratios employed in heavy-load cutting, the bearing surface roughness and hardness must be carefully matched to prevent early failure. This constraint imposes high design requirements on bearings. Future research should focus on exploring advanced surface treatment technologies and coating solutions to further optimize the balance between surface roughness and hardness, particularly for bearings used in high-length-to-diameter-ratio spindles under heavy-load cutting conditions.

Acknowledgements

The author gratefully acknowledges the support of the Shanghai Natural Science Foundation (20ZR1421000).

References

[1] Wang Z, Yin Z C, Wang Z N, et al. Thermal characteristics analysis of bearing in grinding system of grinding robot[C]//IOP Conference Series: Materials Science and Engineering. IOP Publishing, 2023, 1283(1): 012013.

[2] Takabi J, Khonsari M M. On the thermally-induced failure of rolling element bearings[J]. Tribology International, 2016, 94: 661-674..

[3] Zhao Q, Zhao Q, Zhang E, et al. Research on the relationship between thermal aging of lubricating grease outside the contact area of bearing rolling elements and bearing lubrication failure[J]. Engineering Failure Analysis, 2025, 168: 109127.

[4] Bian W, Wang Z, Yuan J, et al. Thermo-mechanical analysis of angular contact ball bearing[J]. Journal of Mechanical Science and Technology, 2016, 30(1): 297-306.

[5] Zhao Y, Han Q, Gao X. Partial wear and deformation of roller bearing under extreme inclined load and its experimental research[J]. Archive of Applied Mechanics, 2023, 93(5): 1879-1899.

[6] Shi X, Lu X, Feng Y, et al. Tribo-dynamic analysis for aero ball bearing with 3D measured surface roughness[J]. Engineering Failure Analysis, 2022, 131: 105848.

[7] Yunlong W, Wenzhong W, Shengguang Z, et al. Effects of raceway surface roughness in an angular contact ball bearing[J]. Mechanism and Machine Theory, 2018, 121: 198-212.

[8] Xi Y, Björling M, Shi Y, et al. Traction formula for rolling-sliding contacts in consideration of roughness under low slide to roll ratios[J]. Tribology International, 2016, 104: 263-271.

[9] Yu J, Zhu S, Yuan W, et al. Investigation on the friction heat generation rate of ball bearings at ultra-high rotation speed[J]. The International Journal of Advanced Manufacturing Technology, 2023, 128(1): 57-79.

[10] Guanci, Chen, Jianmin, et al. Effects of size and raceway hardness on the fatigue life of large rolling bearing[J].Journal of Mechanical Science and Technology, 2015, 29(9):3873-3883.

[11] Trevisiol C, Jourani A, Bouvier S. Effect of hardness, microstructure, normal load and abrasive size on friction and on wear behaviour of 35NCD16 steel[J]. Wear, 2017, 388: 101-111.

[12] Vrček A, Hultqvist T, Baubet Y, et al. Micro-pitting damage of bearing steel surfaces under mixed lubrication conditions: effects of roughness, hardness and ZDDP additive[J]. Tribology International, 2019, 138: 239-249.

[13] Wang C, Aldakheel F, Zhang C, et al. Failure of high-speed bearing at cyclic impact-sliding contacts: Numerical and experimental analysis[J]. International Journal of Mechanical Sciences, 2023, 253: 108410.

[14] Wang H, Lv H, Luo Z. Analysis of Mechanical Properties and Fatigue Life of Microturbine Angular

Contact Ball Bearings under Eccentric Load Conditions[J]. Sensors, 2023, 23(9): 4503.

[15] Masjedi M, Khonsari M M. An engineering approach for rapid evaluation of traction coefficient and wear in mixed EHL[J]. Tribology International, 2015, 92: 184-190.

[16] Liou J L , Lin J F , Liou J L ,et al. A modified fractal microcontact model developed for asperity heights with variable morphology parameters[J].Wear, 2010, 268(1):133-144.

[17] Shen Y L , Tan X H .On the correlation between hardness and yield strength in multilayered elastic-plastic materials[J].Journal of Materials ence, 2005, 40(17):4683-4686.

[18] Del-Río L, Nó M L, Sota A, et al. Internal friction associated with ε martensite in shape memory steels produced by casting route and through additive manufacturing: Influence of thermal cycling on the martensitic transformation[J]. Journal of Alloys and Compounds, 2022, 919: 165806.

[19] Shi Z, Xu H, Wang C, et al. Crack initiation induced by twin-martensite and inclusion in rotatory bending fatigue of a high nitrogen martensite bearing steel[J]. Materials Science and Engineering: A, 2022, 861: 144402.

[20] Goigoux A, Cazottes S, Biboulet N, et al. Surface-initiated rolling contact fatigue on a dent: Microstructural evolutions through failure mechanism[J]. Acta Materialia, 2024, 277: 120201.

[21] Ouyang W, Cheng Q , Jin Y ,et al. Lubrication Performance Distribution of Large Aspect Ratio Water-Lubricated Bearings Considering Deformation and Shaft Bending[J].Tribology Transactions, 2021, 64:730 - 743.

[22] Carrington M J, Daure J L, Utada S, et al. The evolution of subsurface deformation and tribological degradation of a multiphase Fe-based hardfacing induced by sliding contact[J]. Materials Science and Engineering: A, 2024, 892: 146023.

[23] Shahani A R, Babaei M. The crack propagation path for a system of surface and subsurface cracks and their interactions due to rolling contact fatigue[J]. Acta Mechanica, 2020, 231(5): 1751-1764.

[24] Lu G, Zou Y, Chen X, et al. Micro-morphological analysis, lubricating behaviors, and wear failure characteristics and mechanisms of propeller hub bearings in marine environments[J]. Wear, 2023, 530: 205047,

[25] Penghui Y, Hanguang F, Xiangwei Z, et al. Wear behavior of CADI obtained at different austenitizing temperatures[J]. Tribology International, 2019, 140: 105876..

[26] Shi Y, Yao Y, Fei J. Analysis of bulk temperature field and flash temperature for locomotive traction gear[J]. Applied Thermal Engineering, 2016, 99: 528-536.

[27] Wu J, Yang H, Dong P, et al. Effect of various compositions on high-temperature wear failure mechanism of copper-based friction components[J]. Engineering Failure Analysis, 2025, 170: 109275.

[28] Tong X, Han P, Yang S. Study of the friction behavior of AlCrN coated micro-textured surfaces[J]. Tribology International, 2023, 177: 107985.

[29] Yin H, Bai X, Fu H. Prediction of Work Hardening in Bearing Steels Undergoing Rolling Contact Loading with a Dislocation-Based Model[J]. Metals, 2022, 12(4): 555.

[30] Varga M, Badisch E. Temperature and load influence on in-situ formed layers during high

temperature abrasion[J]. Wear, 2017, 384: 114-123.

[31] Feng T, Zhan L, Ma B, et al. Strengthening behavior and microstructure of 2195 Al-Cu-Li alloy under cycling loading[J]. Journal of Alloys and Compounds, 2024, 1005: 176082.

[32] Kang J H, Vegter R H, Rivera-Díaz-del-Castillo P E J. Rolling contact fatigue in martensitic 100Cr6: Subsurface hardening and crack formation[J]. Materials Science and Engineering: A, 2014, 607: 328-333.

[33] Ren J, Li C, Han Y, et al. Effect of initial martensite and tempered carbide on mechanical properties of 3Cr2MnNiMo mold steel[J]. Materials Science and Engineering: A, 2021, 812: 141080.

[34] Saha D C, Biro E, Gerlich A P, et al. Evolution of transient nature nanoscale softening during martensite tempering[J]. Metallurgical and Materials Transactions A, 2020, 51(8): 3772-3777.

[35] Feng Q, Zeng Y, Li J, et al. Effect of Carbides on Thermos-Plastic and Crack Initiation and Expansion of High-Carbon Chromium-Bearing Steel Castings[J]. Metals, 2024, 14(3): 335.

[36] Zhang K, Wang Z B, Lu K. Enhanced fatigue property by suppressing surface cracking in a gradient nanostructured bearing steel[J]. Materials Research Letters, 2017, 5(4): 258-266.

[37] Zhang J, Chen H, Fu H, et al. Retarding effect of submicron carbides on short fatigue crack propagation: Mechanistic modeling and Experimental validation[J]. Acta Materialia, 2023, 250: 118875.

[38] Wang G, Liu H, Tao X, et al. Unraveling the plastic deformation, recrystallization, and oxidation behavior of Waspaloy during thermal fatigue crack propagation[J]. Journal of Alloys and Compounds, 2024, 1004: 175814.

[39] Liu T, Xia Y, Li Y, et al. The combined effects of carbides and martensite blocks heterogeneity on the fatigue life scatter in bearing steel[J]. Materials Science and Engineering: A, 2024, 915: 147277.